

JGR Atmospheres

RESEARCH ARTICLE

10.1029/2019JD031690

Key Points:

- The concentration of stratospheric ozone over the Arctic can be modulated by SSTs in the North Pacific
- Negative SST anomalies in the central North Pacific weaken BD circulation over the Arctic by altering propagation of planetary waves
- The ozone anomalies modulated by SSTs in the the North Pacific are related to the anomalous Brewer–Dobson circulation and the polar vortex

Correspondence to:

D. Hu,
hudz@nuist.edu.cn

Citation:

Liu, M., Hu, D., & Zhang, F. (2020). Connections between Stratospheric Ozone Concentrations over the Arctic and Sea Surface Temperatures in the North Pacific. *Journal of Geophysical Research: Atmospheres*, 125, e2019JD031690. <https://doi.org/10.1029/2019JD031690>

Received 19 SEP 2019

Accepted 24 JAN 2020

Accepted article online 3 FEB 2020

Connections Between Stratospheric Ozone Concentrations Over the Arctic and Sea Surface Temperatures in the North Pacific

Meichen Liu¹ , Dingzhu Hu¹ , and Feng Zhang¹ 

¹Key Laboratory of Meteorological Disasters of China Ministry of Education (KLME)/Joint International Research Laboratory of Climate and Environment Change (ILCEC)/Collaborative Innovation Center on Forecast and Evaluation of Meteorological Disasters (CIC-FEMD), Nanjing University of Information Science & Technology, Nanjing, China

Abstract We examined the relationship between sea surface temperatures (SSTs) in the North Pacific and the concentration of stratospheric ozone in the northern hemisphere in February–March from 1980 to 2017 using reanalysis and satellite datasets. Our results show that the concentration of stratospheric ozone can be modulated by the principle mode of the North Pacific SSTs—that is, there are negative and zonally asymmetrical ozone anomalies in the Arctic stratosphere, but positive ozone anomalies in the lower stratosphere at mid-latitudes during the positive phases of the North Pacific SSTs. The North Pacific SST anomalies account for about 20% of the linear variance of ozone concentrations in the lower stratosphere over the Arctic. Negative SST anomalies in the central North Pacific tend to result in a strengthened Western-Pacific like teleconnection, which favors the propagation of more planetary wavenumber-1 and -2 waves into the stratosphere. The North Pacific SSTs-related upwelling branch of the Brewer–Dobson circulation in the mid-latitude stratosphere strengthens, but its downwelling branch in the Arctic stratosphere weakens. This results in decreased ozone anomalies in the lower stratosphere over the Arctic and increased ozone anomalies in the lower stratosphere at mid-latitudes. The zonally asymmetrical distribution of ozone related to the positive phase of SSTs over the North Pacific may be related to the shifting and strengthening of the stratospheric Arctic vortex.

1. Introduction

The ozone presented in the stratosphere not only shields the Earth from harmful ultraviolet radiation from the Sun (WMO., 2014), but also alters the stratospheric temperature, circulation and wave activities via radiative effects (Hu & Tung, 2003) and radiative–dynamic feedbacks (Coy et al., 1997; Hu et al., 2015; Newman et al., 2001). As a result of the important effects of stratospheric ozone on the Earth's climate, many studies have examined the variabilities in stratospheric ozone and investigated the factors and processes influencing ozone concentrations (e.g., Eyring et al., 2007; Hu et al., 2014; Lu et al., 2019; Weatherhead & Andersen, 2006).

Various factors, including the concentration of greenhouse gases (e.g., Shu et al., 2011; Xie et al., 2008), anthropogenic emissions of ozone-depleting substances (e.g., Weatherhead & Andersen, 2006), the El Niño–Southern Oscillation (ENSO) (e.g., Cagnazzo et al., 2009; Oman et al., 2013; Randel et al., 2009) and the Arctic oscillation (Zhang et al., 2017) have been found to have important roles in the variation of stratospheric ozone. The ENSO can affect the concentration of stratospheric ozone in both the tropics and extratropics (e.g., Cagnazzo et al., 2009; Randel et al., 2009). Decreased temperatures in the tropical lower stratosphere during El Niño events are accompanied by decreased ozone concentrations (Randel et al., 2009; Xie et al., 2012). Cagnazzo et al. (2009) suggested that strong ENSO events lead to warming of the polar vortex and an increase in the column concentration of ozone in the Arctic. However, Hu et al. (2014) showed that an increased meridional gradient of sea surface temperatures (SSTs) over the globe or between 60° S and 60° N could result in increased concentrations of stratospheric ozone over the Arctic, which suggests that extratropical SSTs are also closely related to the concentration of stratospheric ozone.

The relationship between SSTs over the North Pacific and the Arctic vortex in the stratosphere has been investigated in recent years (e.g., Hu et al., 2018; Hu & Guan, 2018; Hurwitz et al., 2011; Jadin et al., 2010; Kren et al., 2016; Rao et al., 2019; Woo et al., 2015). Hurwitz et al. (2011) showed that the

strengthened Arctic vortex in the stratosphere in March 2011 was closely related to warming SSTs in the North Pacific. Woo et al. (2015) reported that there are more weak stratospheric polar vortex events during the positive phases of the Pacific decadal oscillation than in its negative phases. Using a long-term simulation, Kren et al. (2016) confirmed that the polar stratosphere warms and weakens during the positive phases of the Pacific decadal oscillation. Subsequently, Hu and Guan (2018) showed that the stratospheric Arctic vortex strengthens during the positive phases of the Pacific decadal oscillation on a decadal timescale, which is different from their relationship on subdecadal timescales. Hu et al. (2018) reported that ~25% of the strength of the Arctic vortex in the stratosphere is contributed by SSTs in the central North Pacific. Other studies have shown that strong polar vortices always correspond to decreased concentrations of stratospheric ozone, suggesting a connection between the stratospheric Arctic vortex and the concentration of stratospheric ozone (e.g., Douglass et al., 1985; Hartmann, 1981; Hartmann & Garcia, 1979; Randel et al., 2002; Rood & Douglass, 1985). However, few studies have discussed the relationship between the concentration of stratospheric ozone and SSTs in the North Pacific. Hurwitz et al. (2012) used the Goddard Earth Observing System Chemistry–Climate Model (GEOSCCM) to show that warm North Pacific SSTs may lead to a decreased concentration of ozone in the lower stratosphere over the Arctic. Garfinkel et al. (2015) suggested that warming of the North Pacific affected the trend of ozone concentrations in the lower stratosphere and upper troposphere over the polar cap in March from 1980 to 2009. However, the concentration of ozone in the stratosphere over the Arctic exhibits a robust interannual variability (e.g., Kirgis et al., 2013). We therefore need to establish whether there is a connection between the long-term detrended concentration of ozone in the stratosphere over the Arctic and SSTs in the the North Pacific in reanalysis datasets. Although earlier studies have considered the changes in the zonal mean concentration of stratospheric ozone, the relation between the detailed vertical and zonal structure of stratospheric ozone and SSTs in the North Pacific is still unclear.

The Brewer–Dobson circulation (BDC), a meridional circulation in the stratosphere, has a crucial role in the distribution of trace gases, including ozone and water vapor, in the stratosphere. Chipperfield and Jones (1999) suggested that the BDC transports ozone from ozone-rich regions in the tropics to the ozone-poor region in the Arctic stratosphere and that the maximum poleward transport of ozone occurs in the winter months. The changes in ozone concentration as a result of transport by the BDC are effective in the lower stratosphere (Li et al., 2009; Shepherd, 2008). Some studies have confirmed that the speeding up of the BDC as a result of increased concentrations of greenhouse gases could result in a faster recovery of ozone concentrations than the rate predicted by chemical effects alone in chemistry–climate models (Oman et al., 2010). The polar vortex also modulates the distribution of stratospheric ozone. For example, Hu et al. (2014) used chemistry–climate model simulations to show that increased SSTs could lead to increases in the zonal and annual mean concentrations of ozone over the Arctic by weakening the polar vortex in the stratosphere. Zhang et al. (2018) suggested that the Eurasian shift of the polar vortex has resulted in a decrease in the total column ozone over the Eurasian continent during the past three years. The underlying processes between North Pacific SSTs and the concentration of ozone in the stratosphere require further investigation and the relative roles of the Arctic polar vortex and the BDC in the connection between the North Pacific SSTs and concentration of stratospheric ozone are still unclear.

We examined the relationship between stratospheric concentrations of ozone in the Arctic and SSTs in the North Pacific using satellite observations, reanalysis datasets and a chemistry–climate model and investigated the possible dynamic processes. This paper is organized as follows: the data, methods and model are introduced in section 2; the relationship between the concentrations of ozone in the lower stratosphere over the Arctic and SSTs over the North Pacific is analyzed in section 3; the possible dynamic mechanisms between the North Pacific SSTs and lower stratospheric ozone over the Arctic are investigated in section 4; and our discussion and conclusions are presented in section 5.

2. Datasets and Methods

2.1. Datasets

We used the monthly temperature, horizontal and vertical wind velocities, geopotential height and ozone datasets from the National Aeronautics and Space Administration Modern-Era Retrospective Analysis for Research and Applications version 2 (MERRA-2) dataset in the period 1980–2017. This dataset has a

horizontal resolution of $0.5^\circ \times 0.625^\circ$ with 42 pressure levels from the surface to 0.1 hPa (Rienecker et al., 2011). We also used the monthly mean Extended Reconstructed Sea Surface Temperature V5 (ERSST_V5) SST dataset during the period 1980–2017 derived from the International Comprehensive Ocean–Atmosphere Dataset, which has a horizontal resolution of $2^\circ \times 2^\circ$ (Huang et al., 2017). We used ozone records from the Microwave Limb Sounder (MLS) dataset during the period 2005–2017, which is the standard product derived from radiances measured by the 240 GHz radiometer (version 4.2) and covers from 82° S to 82° N (Livesey et al., 2011). We also used the *Oceanic Niño Index* for the period 1980–2017. This index is derived from the National Oceanic and Atmospheric Administration/Earth System Research Laboratory Physical Sciences Division dataset (www.esrl.noaa.gov/psd/data/correlation/oni.data).

2.2. Methods

The two-dimensional quasi-geostrophic Eliassen–Palm flux and its divergence (Edmon et al., 1980), which can be used to measure the strength and propagation of waves, is given as follows:

$$F_\varphi = -a \cos \varphi \overline{\varphi v' u'} \quad (1)$$

$$F_p = \frac{a \cos \varphi f}{d\bar{\theta}/dp} \overline{v' \theta'} \quad (2)$$

$$Div = \frac{1}{a \cos \varphi} \frac{\partial}{\partial \varphi} (F_\varphi \cos \varphi) + \frac{\partial}{\partial p} F_p \quad (3)$$

where F_φ , F_p and Div denote the meridional component, the vertical component and the divergence of the Eliassen–Palm flux, respectively. u and v are the zonal and meridional winds, respectively, and θ is the potential temperature. a is the radius of the Earth, f is the Coriolis parameter, p is the pressure and φ is the latitude. The overbars and primes denote the zonal mean and the departure from the zonal mean, respectively.

Following Monier and Weare (2011), changes in the concentrations of ozone in the lower stratosphere over the Arctic caused by the BDC and eddy transport can be examined via the following equation:

$$\frac{\partial \bar{\chi}}{\partial t} = -\frac{\bar{v}^*}{a} \frac{\partial \bar{\chi}}{\partial \varphi} - \bar{\omega}^* \frac{\partial \bar{\chi}}{\partial z} - \frac{1}{\rho_0} \nabla \cdot \mathbf{M} + \bar{S} \quad (4)$$

where $\bar{\chi}$ is the zonal mean ozone concentration, \bar{v}^* and $\bar{\omega}^*$ are the meridional and vertical transformed Eulerian mean velocities, respectively (Andrews et al., 1987), ρ_0 is the density of air, z is the height and

$\nabla \cdot \mathbf{M}$ is the divergence of the eddy flux vector \mathbf{M} . The components of \mathbf{M} are defined by $\mathbf{M}^{(\varphi)} = \rho_0$

$\left(\overline{v' \chi'} - \frac{\bar{v} \bar{\theta}}{\bar{\theta}_z} \frac{\partial \bar{\chi}}{\partial z} \right)$ and $\mathbf{M}^{(z)} = \rho_0 \left(\overline{\omega' \chi'} + \frac{1}{a} \frac{\bar{v} \bar{\theta}}{\bar{\theta}_z} \frac{\partial \bar{\chi}}{\partial \varphi} \right)$. \bar{S} is the net chemical ozone production term. The other

parameters are the same as in equations (1–3). The first and second terms on the right-hand side of equation (4) represent the advection of ozone by the BDC or the mean transport of ozone. The third term represents the large-scale eddy transport of ozone and the fourth term is the chemical net production of ozone.

According to Birner and Bönisch (2011), the residual stream function is calculated as follows:

$$\bar{\psi}^*(p, \varphi) = \int_0^p \frac{-2 \pi a \cos \varphi \bar{v}^*(p', \varphi)}{g} dp' \quad (5)$$

where $\bar{\psi}^*$ represents the residual stream function and g is the acceleration due to gravity. The other parameters are the same as in equations (1–3).

2.3. Model

To clarify the causal relationship between SSTs over the North Pacific and the average ozone concentration over the polar cap, we designed two sensitivity experiments by adopting the Whole Atmosphere Community Climate Model, version 5 (WACCM5). More details of this model can be found in Garcia et al. (2007) and Marsh et al. (2013). These two 30-year time-slice simulations use a horizontal resolution of $1.9^{\circ} \times 2.5^{\circ}$ (latitude \times longitude). The simulations differ only in the forcing of SSTs over the North Pacific. In the reference run, we used the observed monthly mean climatological SST from the UK Meteorological Office Hadley Centre for the time period 1950–2010. The SSTs in the sensitive run were the same as those in reference run except for the SSTs over the North Pacific (20.5° – 65.5° N, 100° E– 100.5° W). In contrast with the North Pacific SST forcing used in the reference run, the North Pacific SST forcing used in the sensitive run superimposed the SST anomalies (SSTAs), which were obtained as the difference in the SST between stronger positive $PC1_{SST}$ phase ($PC1_{SST} \geq 0.7$) and the stronger negative $PC1_{SST}$ phase ($PC1_{SST} \leq -0.7$) during the time period 1980–2013. $PC1_{SST}$ was the first principal component of the SSTAs over North Pacific obtained by empirical orthogonal function (EOF) analysis.

3. Relationship Between the Levels of Ozone Over the Arctic and SSTs in the North Pacific

The most severe destruction of ozone in the polar regions occurs in late winter and early spring (WMO, 2014) and therefore we focused on the changes in ozone concentrations associated with SSTs over the North Pacific in February–March. To verify the relationship between the concentrations of ozone in the boreal lower stratosphere and SSTs in the northern hemisphere, Figure 1a shows the regression of the SSTAs over the North Pacific on the weighted-average concentrations of ozone over the polar cap from 65 to 90° N at 30–250 hPa in February–March during the time period 1980–2017. The ENSO is an important interannual signal in tropical SSTs and some studies have shown that the ENSO has a relationship with both the SSTAs over the North Pacific and the concentration of ozone in the lower stratosphere (Alexander et al., 2002; Cagnazzo et al., 2009). We therefore removed the linear trend in the SSTAs and stratospheric ozone and then removed the ENSO signals by linear regression. The *Oceanic Niño Index* is used to represent the ENSO. The regression of the SSTAs on the average ozone concentration over the polar cap shows a horseshoe pattern with positive values in the central North Pacific surrounded by significant negative SSTAs in the Gulf of Alaska, off California and toward the tropics (e.g., Bond et al., 2003; Hu et al., 2018).

We subtracted the global mean temperature and then performed an EOF reanalysis of the monthly SSTAs over the North Pacific (100° E– 100.5° W, 20.5° – 65.5° N) following the method of Newman et al. (2016). Figure 1b shows the EOF1 of the monthly SSTAs over the North Pacific derived from the ERSST V5b dataset in February–March during the time period 1980–2017. The first principal component (PC1) accounts for 37.8% of the variance. The maps of SSTAs over the North Pacific regressed on the average ozone concentration over the polar cap (Figure 1a) are very similar to the map of the EOF1 of SSTs over the North Pacific (Figure 1b), which suggests that the concentrations of ozone in the lower stratosphere are closely related to SSTAs over the North Pacific. The correlation coefficient between $PC1_{SST}$ and the weighted-average concentration of ozone over the polar cap is -0.33 , which is statistically significant at the 95% confidence level. This result suggests that there is an out-of-phase relationship between the concentration of ozone in the lower stratosphere over the Arctic and the SSTAs in the North Pacific—that is, the concentration of ozone in the lower stratosphere decreases during positive phases of the SSTAs in the North Pacific and increases during the negative phases of these SSTAs.

To better understand the characteristics of the vertical and meridional structures of the distribution of stratospheric ozone related to SSTAs in the North Pacific, we analyzed the correlation between $PC1_{SST}$ and the zonal mean concentration of ozone in the lower stratosphere over the northern hemisphere during February–March from the MERRA-2 dataset (Figure 2a). $PC1_{SST}$ was positively correlated with the concentration of ozone in the lower stratosphere in mid-latitudes (30 – 100 hPa, 30 – 45° N; hereafter referred to as the “mid-latitude lower stratosphere”), but were negatively correlated in the upper troposphere–lower stratosphere of the Arctic (150 – 250 hPa, 65 – 90° N). The correlation coefficients between $PC1_{SST}$ and ozone in the mid-latitude lower stratosphere and in the Arctic upper troposphere–lower stratosphere were 0.42 and -0.45 , respectively. The latter correlation suggests that changes in $PC1_{SST}$ can account for about 20% of

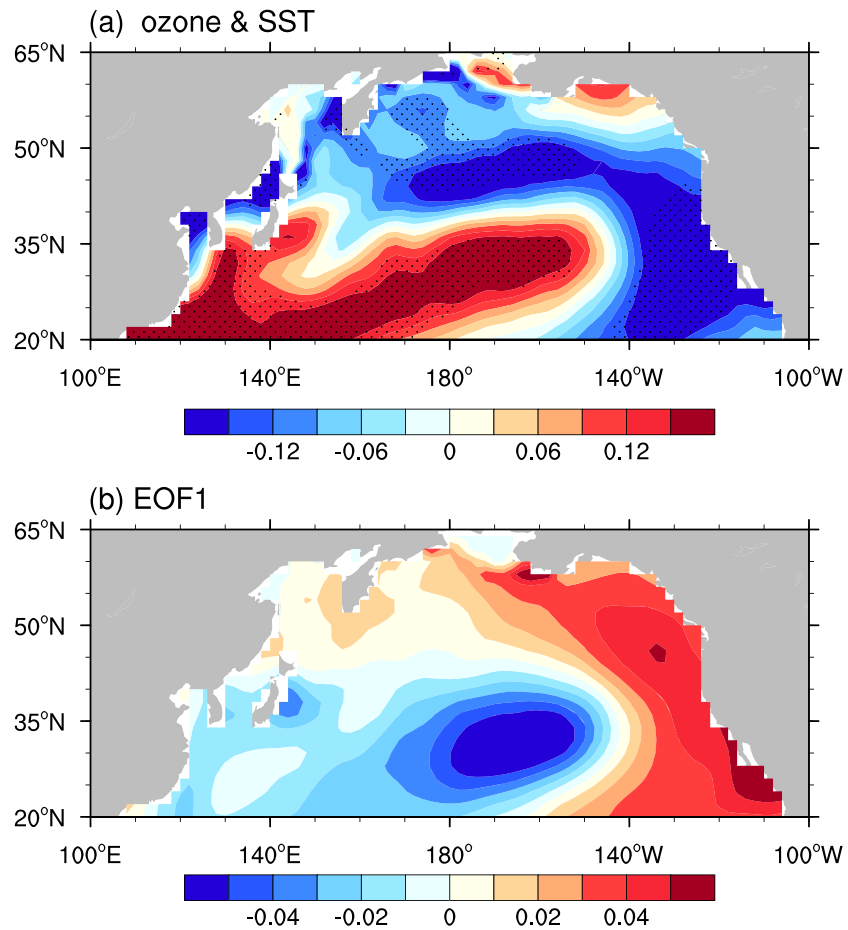


Figure 1. (a) Regression of sea surface temperature anomalies (units: K) over the North Pacific (20.5–65.5° N, 100° E–100.5° W) on the normalized averaged ozone concentration over the polar cap in February–March from 1980 to 2017. The values over the stippled regions are statistically significant at the 90% confidence level. (b) The EOF1 of sea surface temperatures over the North Pacific in February–March from 1980 to 2017.

the linear variance of ozone in the Arctic lower stratosphere. Similar correlation maps between $PC1_{SST}$ and stratospheric ozone concentrations can be seen from MLS satellite measurements (Figure 2b)—that is, there are positive correlations between $PC1_{SST}$ and ozone in the mid-latitude lower stratosphere and negative correlations in the Arctic upper troposphere–lower stratosphere. We further studied the horizontal structures of the distribution of stratosphere ozone related to SSTAs in the North Pacific (Figures 2d, 2e). There were negative correlation coefficients between the $PC1_{SST}$ and stratosphere ozone over the Euro-Atlantic from the MERRA-2 dataset (Figure 2d). Figure 2e shows similar correlations between $PC1_{SST}$ and the concentrations of stratospheric ozone using MLS satellite measurements, in spite of the relatively weak negative correlations over the lower stratosphere of the Arctic derived from the MLS. These results suggest that the out-of-phase relationship between the North Pacific SSTs and the concentrations of ozone in the lower stratosphere over the Arctic is reliable.

To further examine the causal relationship between North Pacific SSTs and the concentration of ozone in the lower stratosphere, we designed two simulations adopting WACCM5 (section 2.3). Figure 2c shows the differences in ozone concentrations in the lower stratosphere between the sensitive and reference runs. There are negative differences in the concentration of ozone in the lower stratosphere over the Arctic. The horizontal pattern of ozone concentrations related to the North Pacific SSTs in Figure 2f shows negative anomalies over the Euro-Atlantic, similar the pattern in Figures 2d and 2e. These results suggest that the positive phase of the SSTAs over the North Pacific could lead to negative anomalies in the concentration of ozone in the

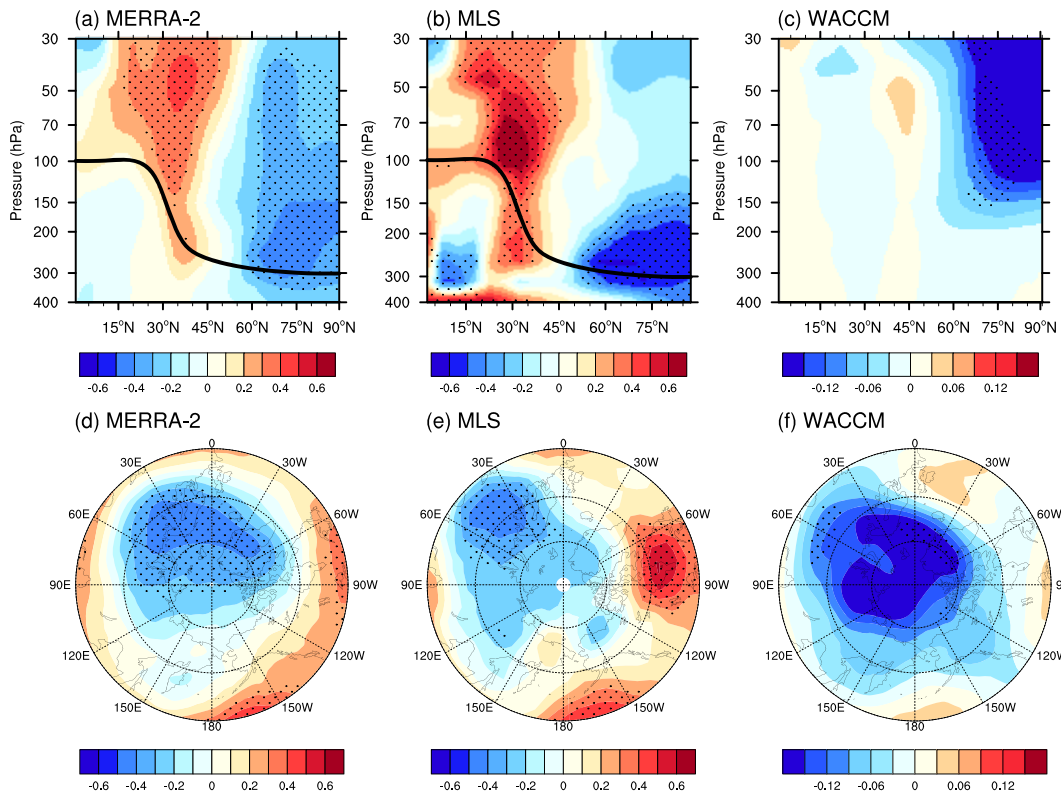


Figure 2. (a) Correlation coefficients between $PC1_{SST}$ and the zonal mean ozone concentration (units: ppmm) in February–March from 400 to 30 hPa over the northern hemisphere using ozone data from (a) the MERRA-2 and (b) MLS datasets. Correlation coefficients between $PC1_{SST}$ and the average ozone concentration from 30 to 250 hPa over the northern hemisphere using ozone data from (d) the MERRA-2 and (e) MLS datasets. The MERRA-2 data cover the time period 1980–2017 and the MLS data cover the time period 2005–2017. (c) Differences in the zonal mean concentration of ozone between the sensitive run and the reference run from 400 to 30 hPa in February–March over the northern hemisphere. (f) Differences in the average concentration of ozone between the sensitive run and the reference run from 30 to 250 hPa in February–March over the northern hemisphere. The values over the stippled regions are statistically significant at the 90% confidence level.

lower stratosphere over the Arctic and also could reproduce the zonally asymmetrical pattern of ozone concentrations.

4. Possible Dynamic Mechanisms

Previous studies have shown that the variability of the concentration of ozone in the upper stratosphere is dominated by chemical processes, but the concentration of ozone in the lower stratosphere is mainly related to dynamic processes (Allen et al., 2012; Solomon et al., 1985). It has been shown that SSTAs over the North Pacific affect the stratospheric Arctic vortex during the boreal winter via dynamic processes (Hu & Guan, 2018; Hurwitz et al., 2012; Rao et al., 2019; Woo et al., 2015). We therefore need to investigate the dynamic mechanisms affecting the concentration of ozone in the lower stratosphere in response to SSTAs over the North Pacific.

4.1. Anomalies in Tropospheric Circulation and Wave Intensity

Planetary wave activities have a key role in changing the circulation in the stratosphere (Christiansen, 2001; Hu et al., 2019; Kuroda & Kodera, 1999). To understand the association of planetary wave activities in the stratosphere with SSTs in the North Pacific, we first analyzed the response of the tropospheric circulation and teleconnection pattern to the North Pacific SST. Many previous studies have shown that the temporal variability of the amplitude of stratospheric planetary waves is affected by the patterns generated in the troposphere (Garfinkel et al., 2010; Randel, 1987). Figure 3a shows the regression of the zonal deviation of the geopotential height and horizontal winds at 500 hPa with respect to $PC1_{SST}$ in February–March during 1980–2017. The geopotential height anomalies over the Pacific related to $PC1_{SST}$ show a teleconnection

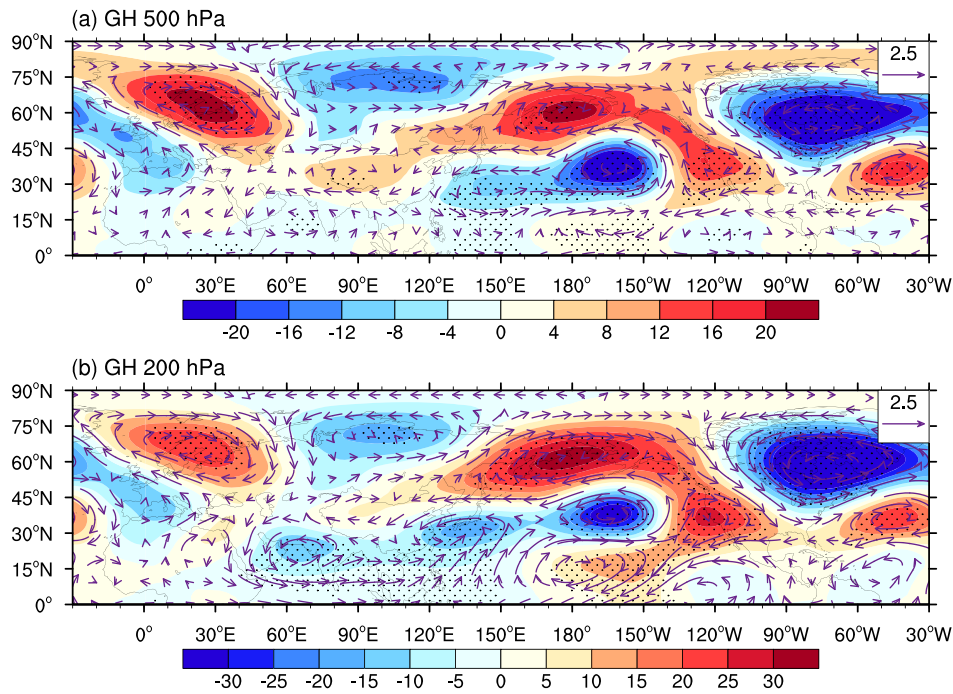


Figure 3. Regression of the zonal deviation of the geopotential height (shading; units: m) and horizontal winds (vectors; units: m s^{-1}) at (a) 500 and (b) 200 hPa with respect to $PC1_{SST}$ in February–March during 1980–2017. The values over the stippled regions are statistically significant at the 90% confidence level.

pattern similar to the Western Pacific pattern, which is consistent with previous studies (e.g., Hu et al., 2018; Wallace & Gutzler, 1981). We calculated the relationship between $PC1_{SST}$ and tropospheric teleconnection patterns following the definitions in Wallace and Gutzler (1981). The correlation coefficient between the Western Pacific teleconnection patterns at 500 hPa and $PC1_{SST}$ is 0.41 and is significant at the 99% confidence level. In addition, a wave train can be clearly seen extending from the North Pacific into the Eurasian continent at mid-latitudes. The horizontal winds at 500 hPa regressed on $PC1_{SST}$ in February–March during 1980–2017 also show alternating anticyclonic and cyclonic anomalies consistent with the geopotential height anomalies. The regressed geopotential height and horizontal winds at 200 hPa (Figure 3b) are in good agreement with those at 500 hPa (Figure 3a). This suggests that there is an equivalent barotropic structure of the wave train pattern in response to the SSTAs over the North Pacific.

The Western Pacific teleconnection pattern has an important role in the wave intensity in the troposphere (Hu & Guan, 2018). Figure 4 shows the anomalies in the zonal deviation of the 200 hPa geopotential height and its wavenumber-1, -2 and -3 components obtained by the regression on $PC1_{SST}$. The anomalies in the zonal deviations of the 200 hPa geopotential height (Figure 4a) show a similar pattern to the anomalies in the wavenumber-2 component (Figure 4c), which suggests that the positive (negative) anomalies in wavenumber-2 of the 200 hPa geopotential height are in phase with its climatology. The anomalies in the wavenumber-1 component are opposite in phase to its climatology (Figure 4b) and are accompanied by the positive (negative) wavenumber-3 component anomalies co-located with its positive (negative) climatology (Figure 4d). The magnitude of the wavenumber-3 component is much smaller than that of wavenumbers-1 and -2, which implies that the contribution of the wavenumber-3 component to the total wave intensity in the upper troposphere is much smaller than that of wavenumbers-1 and -2. These results show that the wave intensity of planetary wavenumber-1 related to $PC1_{SST}$ in the upper troposphere weakens, but the wave intensity of wavenumbers-2 and -3 strengthens. The total wave intensity in the troposphere is jointly contributed by the weakened intensity of wavenumber-1 and the strengthened intensity of wavenumber-2.

4.2. Anomalies in Stratospheric Wave Activity

The tropospheric teleconnection associated with the North Pacific SSTAs could affect the stratosphere wave intensity by changing the tropospheric wave intensity. The planetary wave in the stratosphere has a key role

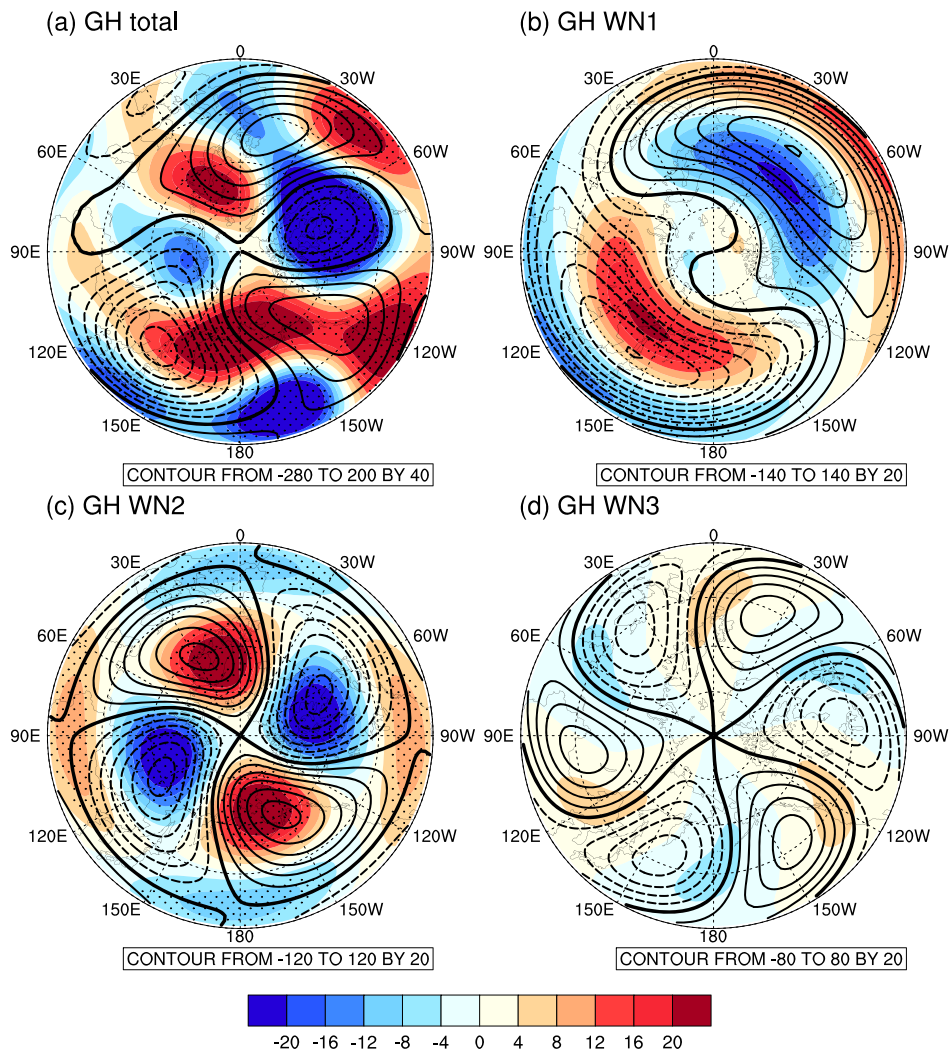


Figure 4. Anomalies (shading) in the (a) zonal deviation of the 200 hPa geopotential height, its (b) wavenumber-1, (c) wavenumber-2 and (d) wavenumber-3 components regressed on $PC1_{SST}$ in February–March from 1980 to 2017. The solid and dashed contours represent the positive and negative climatology of (a) the zonal deviation of the 200 hPa geopotential height and its (b) wavenumber-1, (c) wavenumber-2 and (d) wavenumber-3 components, respectively. The values over the stippled regions are statistically significant at the 90% confidence level.

in stratospheric circulation (Hurwitz et al., 2012; Orsolini et al., 2009). To examine the wave activity in the stratosphere, Figure 5 shows the anomalies in the zonal deviation of the 50 hPa geopotential height and its wavenumber-1, -2 and -3 components obtained by regression on $PC1_{SST}$. The spatial pattern of the anomalies in its wavenumber-1 component (shading in Figure 5b) is similar to that of the total wave activity (Figure 5a). Although the anomalies in the wavenumber-1 component of the geopotential height look mostly in quadrature with its climatologies at mid-latitudes, the anomalous wavenumber-1 component from 65 to 90° N shows a wavenumber-1-like pattern in phase with its climatologies (contours) (Figure 5b), which suggests strengthened wavenumber-1 wave activity in the high-latitude stratosphere. The quadrature area is mainly located at mid-latitudes, which is possibly related to the increased upward propagation of wavenumber-2 of the Eliassen–Palm flux in Figure 7c, which shows the anomalies in the wavenumber-2 component of the Eliassen–Palm flux regressed on $PC1_{SST}$. This may be because there is a clear pathway for the upward propagation of wavenumber-2 at latitudes south of 65° N from the upper troposphere into the stratosphere (Figure 7c). The magnitude of the negative (positive) center of the anomalous total geopotential height from 65 to 90° N is smaller (larger) than that of wavenumber-1, which may be a result of the contributions from wavenumber-2 (Figure 5c). Because the

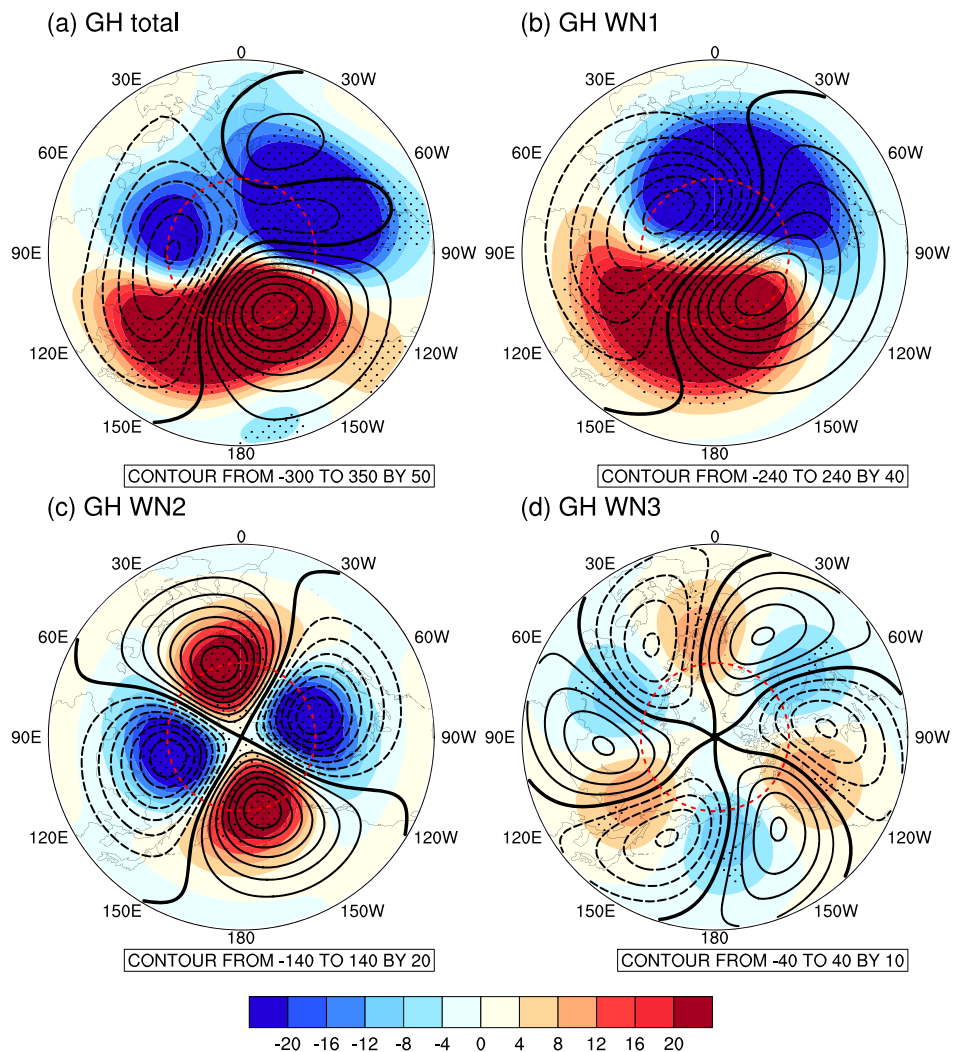


Figure 5. Anomalies (shading) in the (a) zonal deviations of 50 hPa geopotential height and its (b) wavenumber-1, (c) wavenumber-2 and (d) wavenumber-3 components regressed on $PC1_{SSST}$ in February–March from 1980 to 2017. The solid and dashed contours represent the positive and negative climatology of (a) the zonal deviation of the 50 hPa geopotential height and its (b) wavenumber-1, (c) wavenumber-2 and (d) wavenumber-3 components, respectively. The values over the stippled regions are statistically significant at the 90% confidence level. The red circle is the location of 65°N.

magnitude of the climatological wavenumber-1 is much larger than that of wavenumber-2, the wave activity north of 65° N still shows a pattern similar to that of wavenumber-1, consistent with the upward propagation of the wavenumber-1 component of the Eliassen–Palm flux in this region (Figure 7b).

Figure 6 shows the longitude–pressure cross-sections of the regressed zonal deviation of the geopotential height averaged over 55–65 and 65–75° N and its wavenumber-1 and -2 components based on $PC1_{SSST}$. The total anomalies in the geopotential height averaged over 55–65 and 65–75° N related to $PC1_{SSST}$ both show a similar pattern to wavenumber-2 over 300–100 hPa (Figures 6a and 6d), suggesting the importance of wavenumber-2 at these levels. Above 100 hPa, the total anomalies in the geopotential height (shading in Figures 6a and 6d) are more like a wavenumber-1 pattern, with one negative center over the Atlantic Ocean and one positive center over the Pacific Ocean. The latitudes of the positive and negative centers of the anomalous total and wavenumber-1 component of geopotential height averaged over 55–65° N related to $PC1_{SSST}$ (shading in Figures 6a–6c) are nearly the same as those averaged over 65–75° N (Figures 6d–6f), except for the wavenumber-2 component averaged over 55–65° N with an eastward shift (Figure 6c). However, if we compare the climatologies in the geopotential height averaged over 55–65° N with that averaged over 65–75° N, the positive center of the total climatological geopotential height (contours) averaged

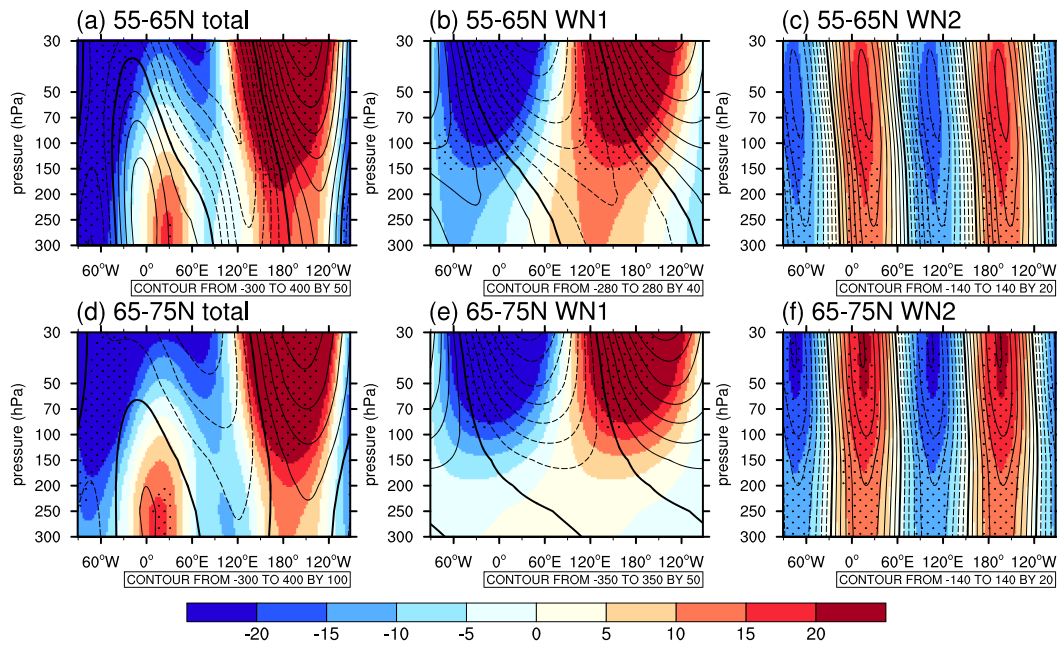


Figure 6. Anomalies (shading) in the (a) zonal deviation of the average geopotential height at 55–65° N and its (b) wavenumber-1 and (c) wavenumber-2 components regressed on $PC1_{SST}$ in February–March from 1980 to 2017. Solid and dashed contours represent the positive and negative climatology of (a) the zonal deviation of the average geopotential height at 65–75° N and its (b) wavenumber-1 and (c) wavenumber-2. Anomalies (shading) in the (d) zonal deviation of the average geopotential height at 65–75° N and its (e) wavenumber-1 and (f) wavenumber-2 components regressed on $PC1_{SST}$. The values over the stippled regions are statistically significant at the 90% confidence level.

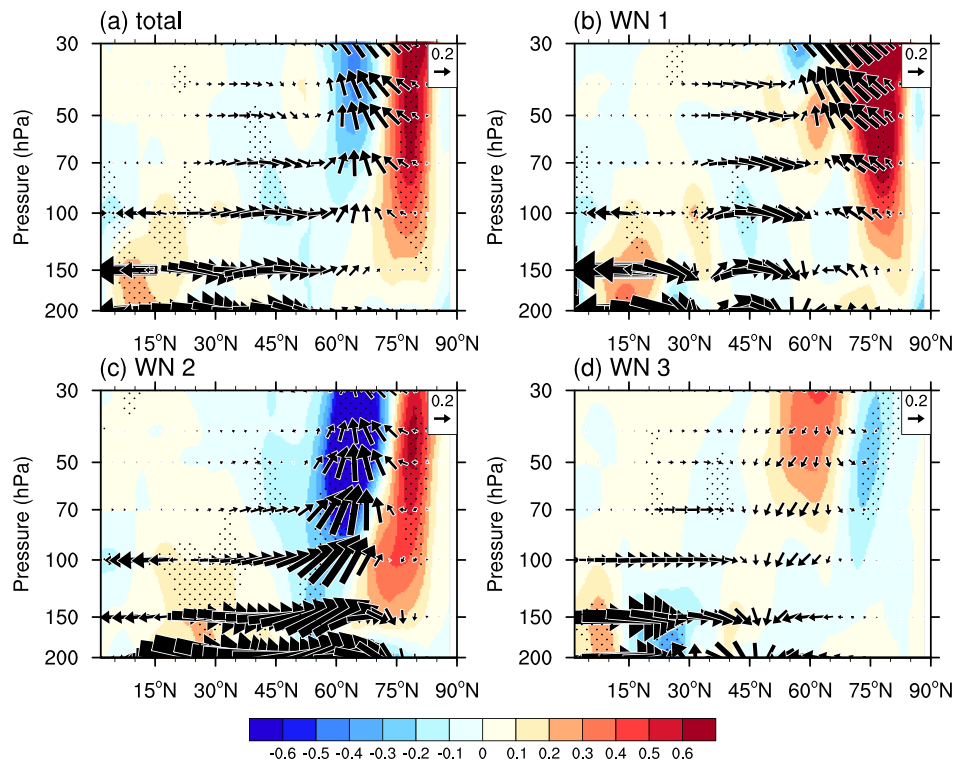


Figure 7. Regressions of the (a) Eliassen–Palm flux (arrows with units of 10^5 kg s^{-2} for vertical vectors and 10^7 kg s^{-2} for horizontal vectors) and Eliassen–Palm flux divergence (shading) and its (b) wavenumber-1, (c) wavenumber-2 and (d) wavenumber-3 components on $PC1_{SST}$ in February–March from 1980 to 2017. The vertical and horizontal Eliassen–Palm flux are multiplied by $\sqrt{\frac{1000}{p}}$. The values over the stippled regions are statistically significant at the 90% confidence level.

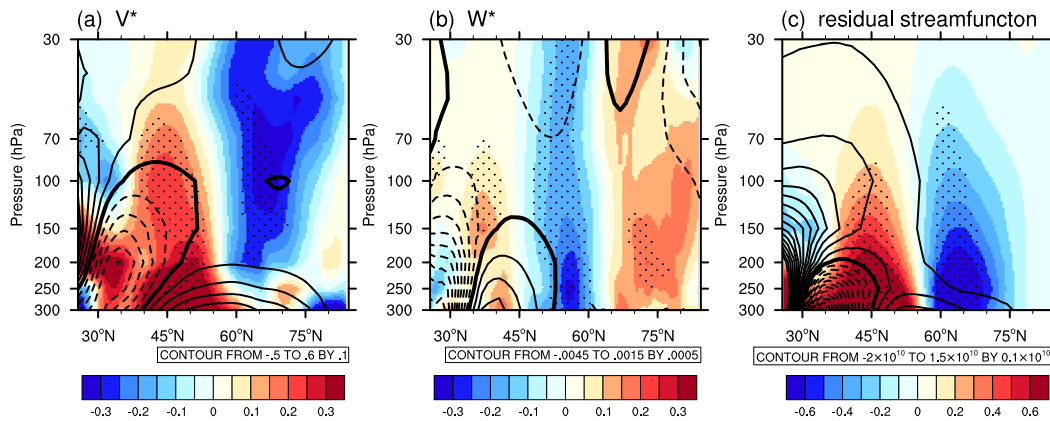


Figure 8. Regression of the (a) v^* (10^{-1} m s^{-1}), (b) w^* (10^{-3} m s^{-1}) and (c) residual streamfunction anomalies (10^9 kg s^{-1}) on $PC1_{SST}$ in February–March from 1980 to 2017. The dashed and solid contours represent the negative and positive, respectively, climatological mean of v^* , w^* and the residual streamfunction. The values over the stippled regions are statistically significant at and above the 90% confidence level.

over $55\text{--}65^\circ \text{ N}$ in the Pacific Ocean has shifted slightly eastward (Figure 6a), accompanied by a slightly eastward shift in its climatological wavenumbers-1 (Figure 6b) and -2 (Figure 6c). These results suggest that the mean circulations to the south of 65° N and the north of 65° N are slightly different, which may be why the anomalies in the wavenumber-1 component of the geopotential height appear mostly in quadrature with its climatologies. The shift in the mean circulation averaged over $55\text{--}65^\circ \text{ N}$ (Figures 6a–6c) is possibly caused by the increased upward propagation of the wavenumber-2 waves (Figure 7). This needs further investigation.

Figure 7 shows the anomalies in the Eliassen–Palm flux and its divergence and the wavenumber-1, -2, and -3 components regressed on $PC1_{SST}$ in February–March during 1980–2017. The Eliassen–Palm flux related to $PC1_{SST}$ shows strengthened anomalies in the stratosphere (Figure 7a), accompanied by a divergence anomaly in the Eliassen–Palm flux divergence at high latitudes. Consistent with the total Eliassen–Palm flux and its divergence, the wavenumber-1 and -2 components of the Eliassen–Palm flux regressed on $PC1_{SST}$ both show anomalous strengthened upward propagation into the extratropical stratosphere and their positive Eliassen–Palm flux divergence related to $PC1_{SST}$ is statistically significant over the polar region (Figures 7b and 7c). The wavenumber-1 wave propagation related to $PC1_{SST}$ appears weaker than the wavenumber-2 propagation at mid-latitudes, but appears stronger than the wavenumber-2 propagation at high latitudes (Figures 7b and 7c). Anomalies in the wavenumber-3 components of the Eliassen–Palm flux and its divergence (Figure 7d) are much smaller than the anomalies in the wavenumber-1 and -2 components.

4.3. Anomalies in Stratospheric Wave Activity

Changes in the planetary waves in the lower stratosphere may lead to an anomalous BDC (e.g., Hu et al., 2014, 2017), which is closely related to the concentration of ozone in the stratosphere (e.g., Hu et al., 2015, 2017; Jiang et al., 2007). Figures 8a and 8b show the regression of v^* and w^* of the BDC on the $PC1_{SST}$. There are negative anomalies in v^* and positive anomalies in w^* in the lower stratosphere of the Arctic during the positive phases of $PC1_{SST}$, which are out-of-phase with their climatology, indicating a weakened downwelling of the BDC over the Arctic during the positive phases of $PC1_{SST}$. The anomalies in the velocities of BDC related to $PC1_{SST}$ at mid-latitudes are different from those over the Arctic—that is, the positive anomalies of v^* and the negative anomalies of w^* are in phase with their climatology, which implies a strengthened upwelling of the BDC in the lower stratosphere at mid-latitudes. Consistent with the velocities of the BDC, the residual stream function related to $PC1_{SST}$ shows negative anomalies at high latitudes and positive anomalies at mid-latitudes (Figure 8c). The response of the BDC to the SSTAs over the North Pacific at mid- and high latitudes are consistent with the convergence and divergence anomalies in the Eliassen–Palm flux divergence at mid- and high latitudes in the stratosphere (Figure 7).

Figure 9 shows the response of the four terms in equation (4) to the SSTAs over the North Pacific. There are positive ozone anomalies in the lower stratosphere of the Arctic and negative ozone anomalies at mid-latitudes related to the anomalous meridional BDC (Figure 9a). These anomalies could be a result of a

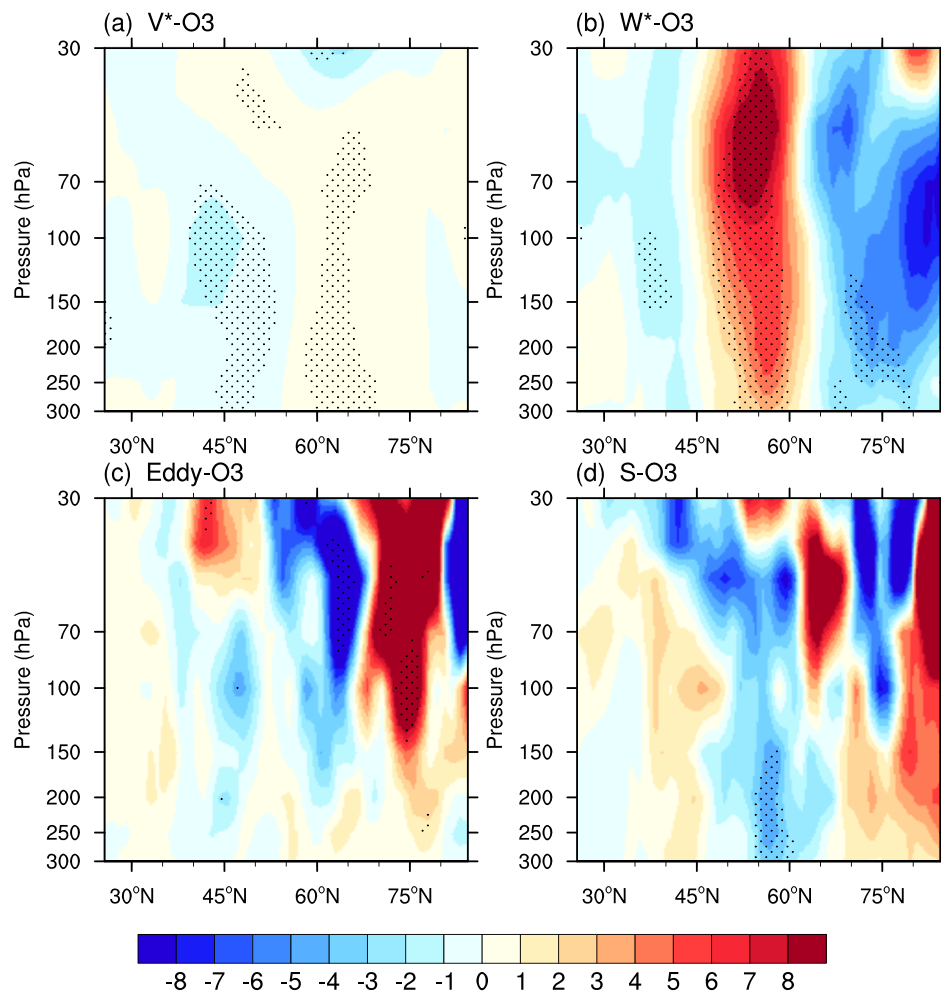


Figure 9. Regression of the ozone anomalies produced by (a) v^* (ppbm day^{-1}), (b) w^* (ppbm day^{-1}), Eddy (ppbm day^{-1}) and S (ppbm day^{-1}) on $PC1_{SST}$ in February–March from 1980 to 2017. The values over the stippled regions are statistically significant at and above the 90% confidence level.

reduction in transport from the ozone-poor Arctic to the ozone-rich mid-latitude regions. Accordingly, the decreased w^* tends to result in negative ozone anomalies in the lower stratosphere Arctic (Figure 9b) by weakening transport from the ozone-rich region in the mid-stratosphere to the ozone-poor region in the lower stratosphere. However, the net ozone anomalies depend on vertical transport by the BDC. The ozone anomalies related to $PC1_{SST}$ caused by eddy transport are positive in the Arctic stratosphere (Figure 9c), which means that eddy transport may increase the concentration of ozone there, which is not consistent with the decreased concentration of ozone associated with the SSTAs in the North Pacific. The net chemical processes related to $PC1_{SST}$ tend to result in non-significant positive ozone anomalies over the lower stratosphere of the Arctic and non-significant negative ozone anomalies over the mid-stratosphere of the Arctic (Figure 9d).

BrO and ClO are the main chemicals that can deplete ozone in early spring (WMO., 2014). We therefore used the concentrations of BrO and ClO measured by the MLS to check the chemical source term directly (figure not shown). The anomalies in the concentrations of BrO and ClO related to $PC1_{SST}$ were statistically insignificant, which further indicates the minor contribution of chemical effects on the concentration of ozone. These results suggest that the BDC terms related to the North Pacific SSTAs play a key part in determining the changes in ozone concentration, but also that the eddy transport and chemical processes related to the SSTAs in the North Pacific may modulate the concentration of ozone. The residual term actually contains three terms that modify the ozone concentration: chemical production; molecular diffusion; and gravity

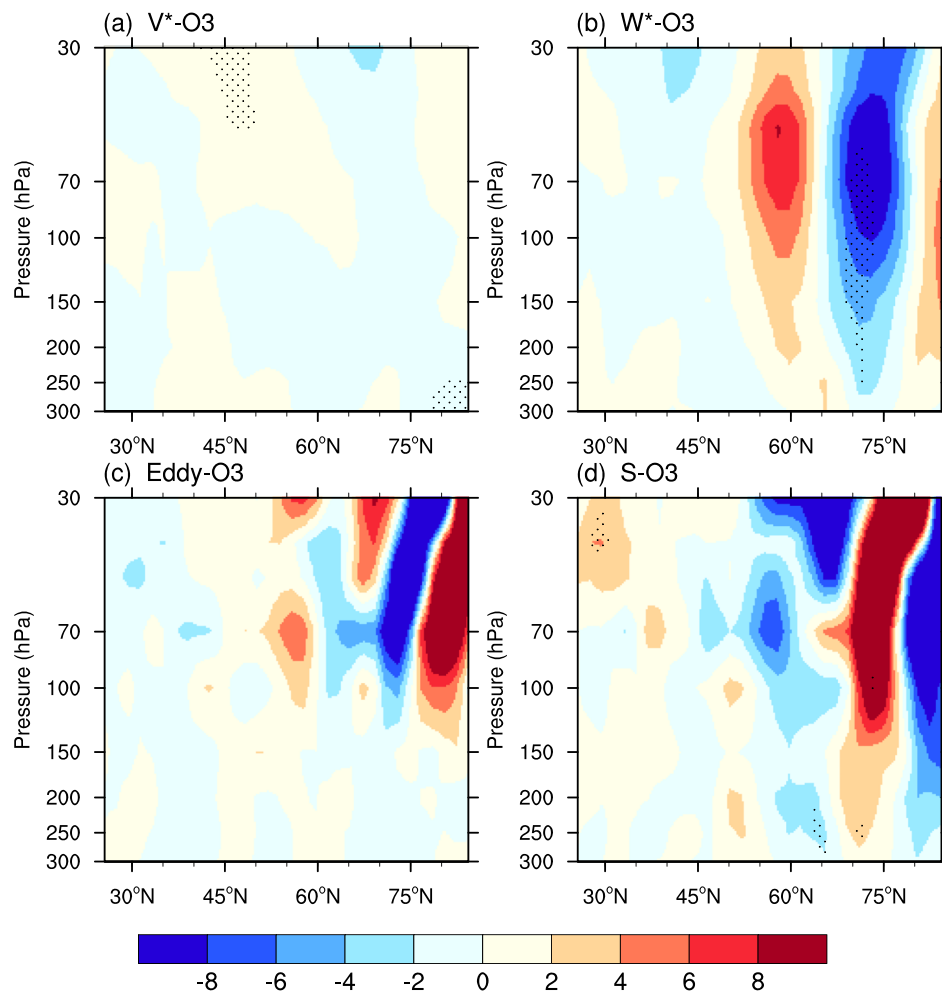


Figure 10. Differences of the ozone anomalies produced by (a) v^* (ppbm day^{-1}), (b) w^* (ppbm day^{-1}), Eddy (ppbm day^{-1}) and S (ppbm day^{-1}) between the sensitive run and the reference run from 300 to 30 hPa in February–March over the northern hemisphere. The values over the stippled regions are statistically significant at and above the 90% confidence level.

waves (Ryan et al., 2018). Ryan et al. (2018) showed that the magnitudes of the gravity wave and molecular diffusion terms are smaller than the chemical processes term in the northern hemisphere. The residual term in equation (4) may be an approximation of the net chemical production term. Some previous studies have suggested that gravity waves could affect polar stratospheric clouds via small-scale temperature fluctuations and that the polar stratospheric clouds induced by gravity waves in the northern hemisphere are non-uniform in the meridional direction (Alexander et al., 2013; Hoffmann et al., 2017; Zhao et al., 2019). The meridional structure of the residual term in Figure 9d is therefore possibly related to the modulation of stratospheric ozone concentrations by gravity waves and molecular diffusion.

Figure 10 shows the budget from the WACCM simulations. The structure of the ozone anomalies related to w^* and the eddies induced by the warmed North Pacific SSTs (Figures 10b and 10c) is similar to the results from the reanalysis datasets (Figure 9). Both the reanalysis datasets and the WACCM simulations suggest a minor contribution of v^* to the ozone anomalies. The residual term in the WACCM simulations (Figure 10d) is not close to zero, which means that the budget in WACCM is close. The magnitude of the residual term from WACCM is consistent with that from the reanalysis datasets, although there are some discrepancies between the results from the reanalysis datasets and the model. This may be related to the parameterization scheme of the gravity wave in the WACCM simulation (Garcia et al., 2017; Smith et al., 2014).

We examined the effect of the meridional and vertical BDC on the ozone anomalies in the stratosphere. Figure 11 shows the regression of the sum of the ozone anomalies transported by the meridional and

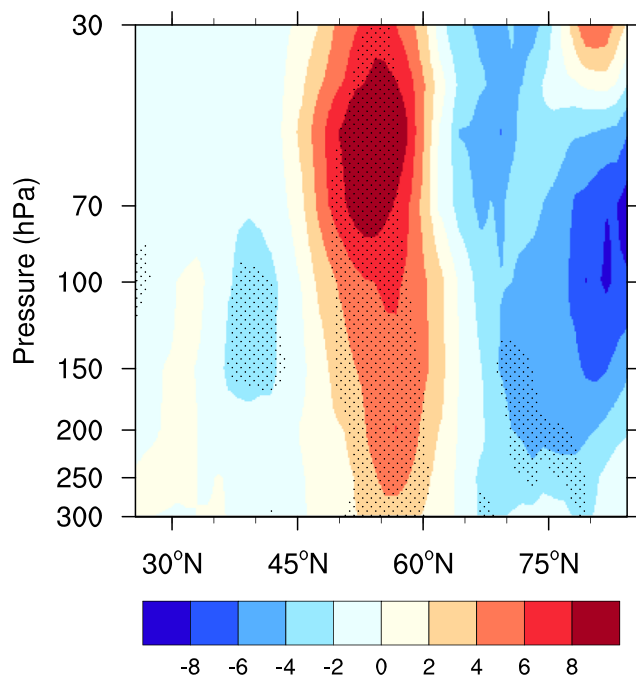


Figure 11. Regression of the sum of the ozone anomalies (ppbm day^{-1}) produced by v^* and w^* on $PC1_{SST}$ in February–March from 1980 to 2017. The values over the stippled regions are statistically significant at and above the 90% confidence level.

vertical BDC with respect to $PC1_{SST}$ in February–March during the time period 1980–2017. There are positive ozone anomalies at mid-latitudes and negative ozone anomalies in the lower stratosphere of the Arctic. The distribution of the ozone transported by the BDC is consistent with previous results (Figures 2a and 2b). By considering Figures 8–11 together, we can see that the SSTAs over the North Pacific tend to result in decreased ozone concentrations in the lower stratosphere over the Arctic and increased ozone concentrations in the lower stratosphere at mid-latitudes by changing the BDC.

The stratospheric polar vortex could also influence the concentration of ozone in the stratosphere (e.g., Hu et al., 2015; Zhang et al., 2018). Following Nash et al. (1996), we defined the edge of the polar vortex as the location of the maximum gradient of Ertel's potential vorticity, which is constrained by the location of the maximum jet calculated along the isolines of Ertel's potential vorticity. Figure 12 shows the anomalies in the potential vorticity between the positive and negative phases of the SSTAs over the North Pacific. The criterion for strong positive (negative) SSTAs over the North Pacific is a normalized $PC1_{SST}$ from 1980 to 2017 greater than 0.8 (less than -0.8). According to this criterion, the positive SSTA years are 1986, 1996, 2014 and 2015, whereas the negative SSTA years are 1988, 1990, 1999, 2002 and 2012. In isentropic coordinates, the areas with a high potential vorticity represent air coming from the polar region (Zhang et al., 2018). There are positive potential vorticity anomalies over the Euro-Atlantic during the positive phase of SSTAs over the North Pacific (Figure 12), which suggests that the polar vortex shifted toward the Euro-Atlantic region. The edge of the polar vortex during the

positive SSTA years is wider than that during the negative years, which suggests that the polar vortex has a strengthened and shifted anomaly during the positive SSTAs years. Anomalies in the edge of the polar vortex related to the North Pacific SSTs are consistent with the zonal distribution of ozone shown in Figure 2. This means that the SSTAs over the North Pacific tend to result in decreased ozone concentrations in the lower stratosphere over the Arctic via weakening of the BDC (Figures 8–11) and the asymmetrical distribution of the concentration of ozone is related to strengthening and shifting of the response of the polar vortex to SSTAs over the North Pacific (Figure 12).

5. Discussion and Conclusions

This study examined the connections between SSTs over the North Pacific and the zonal mean concentration of ozone in the lower stratosphere over the northern hemisphere in February–March using the MERRA-2 and MLS datasets. We found that the correlation coefficients between the principle mode of the North Pacific SSTAs and ozone concentrations in the lower stratosphere at mid-latitudes and over the lower stratosphere in the Arctic are 0.42 and -0.45 , respectively. This means that the concentration of stratosphere ozone is decreasing over the Arctic during the positive phase of SSTAs over the North Pacific, but increasing at mid-latitudes. These results confirm that the SSTs over the North Pacific could lead to a decrease in ozone in the lower stratosphere over the Arctic.

Further investigations showed that the concentrations of ozone in the lower stratosphere over the northern hemisphere related to the North Pacific SSTAs are mainly contributed by the associated dynamic processes. The positive phases of the leading mode of the North Pacific SSTAs tend to result in a strengthened teleconnection similar to the Western Pacific teleconnection and an equivalent barotropic wave train at mid-latitudes extending from the North Pacific into the Eurasian continent, accompanied by more planetary wavenumber-1 and -2 waves propagated into the stratosphere. The strengthened wave activity in the stratosphere tends to strengthen the upwelling branch of the BDC in the lower stratosphere at mid-latitudes and to weaken the downwelling branch of the BDC in the lower stratosphere of the Arctic. Changes in the BDC associated with the North Pacific SSTAs result in decreased ozone concentrations in the lower

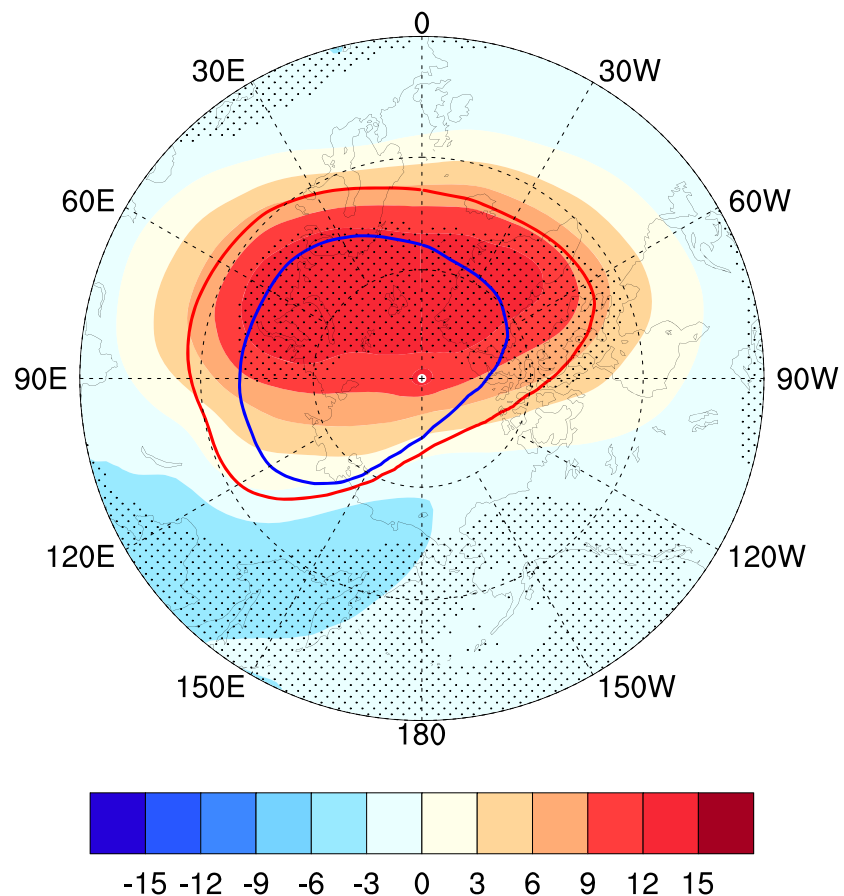


Figure 12. Difference of potential vorticity anomalies (units: $10^6 \text{ K m}^2 \text{ kg}^{-1} \text{ s}^{-1}$) between the positive and negative phase of $PC1_{SST}$ in February–March from 1980 to 2017. The red (blue) line contours represent the polar vortex related to the positive (negative) phase of $PC1_{SST}$ averaged over the isentropic layers from 430 to 600 K. The stippled regions show the values significant at the 90% level.

stratosphere of the Arctic and increased ozone concentrations in the lower stratosphere at mid-latitudes via vertical transportation. In addition, the asymmetrical distribution of the concentration of ozone is related to the strengthening and shifting of the response of the polar vortex to SSTAs over the North Pacific.

Hurwitz et al. (2012) examined the relationship between SSTs over the North Pacific and the concentration of ozone in the stratosphere. Using a chemistry–climate model, they found that the concentration of ozone in the lower stratosphere of the Arctic is related to SSTs in the North Pacific. Our results are partly consistent with theirs, but the datasets, scope and the methodology in our work differs, and we also use a different chemistry-climate model WACCM5 to investigate the relationship between the SSTs over the North Pacific and the concentration of stratosphere ozone. Our studies focused more on the details of the dynamic processes between the North Pacific SSTAs and the concentration of stratospheric ozone, especially the roles of the BDC and the shift in the polar vortex.

The planetary waves associated with the SSTAs over the North Pacific may also affect the concentration of ozone by producing an anomalous temperature in the stratosphere of the Arctic, which is an important condition for the chemical processes related to the depletion of ozone (Barnett et al., 1975; Craig & Ohring, 1958). Previous studies have shown that gas phase ozone loss reactions in the upper stratosphere are dependent on temperature and that a negative temperature anomaly leads to a positive ozone anomaly. Brasseur and Solomon (2005) showed that this negative ozone–temperature feedback is relatively weak in the lower stratosphere. Our results suggest that the concentration of ozone in the lower stratosphere is closely related to the dynamic processes associated with the SSTAs. This is useful in predicting the concentrations of ozone in the Arctic region.

Acknowledgments

We appreciate three anonymous reviewers and editor for their valuable comments and suggestions. We are grateful to the groups and agencies for providing the datasets used in this study. The MERRA-2 reanalysis datasets used here were obtained online from <https://disc.gsfc.nasa.gov/datasets?keywords=MERRA-2>. The ozone datasets from MLS are available at https://disc.gsfc.nasa.gov/datasets/ML2O3_V004/summary?keywords=MLS. The ERSST_V5 from ICOADS is downloaded from <https://www.esrl.noaa.gov/psd/data/gridded/data.noaa.ersst.v5.html>. The Oceanic Niño index is derived from <https://www.esrl.noaa.gov/psd/data/correlation/oni.data>. This work was supported jointly by the National Natural Science Foundation of China (41805031, 41675003, and 41705057).

References

- Alexander, M. A., Bladé, I., Newman, M., Lanzante, J. R., Lau, N., & Scott, J. D. (2002). The Atmospheric Bridge: The Influence of ENSO Teleconnections on Air–Sea Interaction over the Global Oceans. *Journal of Climate*, *15*(16), 2205–2231. [https://doi.org/10.1175/1520-0442\(2002\)015<2205:TABTIO>2.0.CO;2](https://doi.org/10.1175/1520-0442(2002)015<2205:TABTIO>2.0.CO;2)
- Alexander, S. P., Klekociuk, A. R., McDonald, A. J., & Pitts, M. C. (2013). Quantifying the role of orographic gravity waves on polar stratospheric cloud occurrence in the Antarctic and the Arctic. *Journal of Geophysical Research: Atmospheres*, *118*, 11,411–493,507. <https://doi.org/10.1002/2013JD020122>
- Allen, R. J., Sherwood, S. C., Norris, J. R., & Zender, C. S. (2012). Recent Northern Hemisphere tropical expansion primarily driven by black carbon and tropospheric ozone. *Nature*, *485*(7398), 350–354. <https://doi.org/10.1038/nature11097>
- Andrews, D. G., Holton, J. R., & Leovy, C. B. (1987). *Middle Atmosphere Dynamics* (p. 489). San Diego, CA: Academic Press Inc.
- Barnett, J. J., Houghton, J. T., & Pyle, J. A. (1975). The temperature dependence of the ozone concentration near the stratopause. *Quarterly Journal of the Royal Meteorological Society*, *101*(428), 245–257. <https://doi.org/10.1002/qj.49710142808>
- Birner, T., & Bönisch, H. (2011). Residual circulation trajectories and transit times into the extratropical lowermost stratosphere. *Atmospheric Chemistry and Physics*, *11*(2), 817–827. <https://doi.org/10.5194/acp-11-817-2011>
- Bond, N. A., Overland, J. E., Spillane, M., & Stabeno, P. (2003). Recent shifts in the state of the North Pacific. *Geophysical Research Letters*, *30*(23), 2183. <https://doi.org/10.1029/2003GL018597>
- Brasseur, G. P., & Solomon, S. (2005). *Aeronomy of the middle atmosphere: Chemistry and physics of the stratosphere and mesosphere* (p. 2005). Dordrecht, Holland: D. Reidel Publishing Company.
- Cagnazzo, C., Manzini, E., Calvo, N., Douglass, A. R., Akiyoshi, H., Bekki, S., et al. (2009). Northern winter stratospheric temperature and ozone responses to ENSO inferred from an ensemble of Chemistry Climate Models. *Atmospheric Chemistry and Physics*, *9*(22), 8935–8948. <https://doi.org/10.5194/acp-9-8935-2009>
- Chipperfield, M. P., & Jones, R. L. (1999). Relative influences of atmospheric chemistry and transport on Arctic ozone trends. *Nature*, *400*(6744), 551–554.
- Christiansen, B. (2001). Downward propagation of zonal mean zonal wind anomalies from the stratosphere to the troposphere: Model and reanalysis. *Journal of Geophysical Research*, *106*(D21), 27,307–27,322. <https://doi.org/10.1029/2000JD000214>
- Coy, L., Nash, E. R., & Newman, P. A. (1997). Meteorology of the polar vortex: Spring 1997. *Geophysical Research Letters*, *24*(22), 2693–2696. <https://doi.org/10.1029/97GL52832>
- Craig, R. A., & Ohring, G. (1958). The temperature dependence of ozone radiational heating rates in the vicinity of the mesopause. *Journal of Meteorology*, *15*(1), 59–62. [https://doi.org/10.1175/1520-0469\(1958\)015<0059:TTDOOR>2.0.CO;2](https://doi.org/10.1175/1520-0469(1958)015<0059:TTDOOR>2.0.CO;2)
- Douglass, A. R., Rood, R. B., & Stolarski, R. S. (1985). Interpretation of ozone temperature correlations: 2. Analysis of SBUV ozone data. *Journal of Geophysical Research*, *90*(D6), 10,693–10,708. <https://doi.org/10.1029/JD090iD06p10693>
- Edmon, H. J., Hoskins, B. J., & McIntyre, M. E. (1980). Eliassen–Palm Cross Sections for the Troposphere. *Journal of the Atmospheric Sciences*, *37*(12), 2600–2616. [https://doi.org/10.1175/1520-0469\(1980\)037<2600:EPCSFT>2.0.CO;2](https://doi.org/10.1175/1520-0469(1980)037<2600:EPCSFT>2.0.CO;2)
- Eyring, V., Waugh, D. W., Bodeker, G. E., Cordero, E., Akiyoshi, H., Austin, J., et al. (2007). Multimodel projections of stratospheric ozone in the 21st century. *Journal of Geophysical Research*, *112*, D16303. <https://doi.org/10.1029/2006JD008332>
- García, R. R., Marsh, D. R., Kinnison, D. E., Boville, B. A., & Sassi, F. (2007). Simulation of secular trends in the middle atmosphere, 1950–2003. *Journal of Geophysical Research*, *112*, D09301. <https://doi.org/10.1029/2006JD007485>
- García, R. R., Smith, A. K., Kinnison, D. E., Cámara, Á. D. L., & Murphy, D. J. (2017). Modification of the Gravity Wave Parameterization in the Whole Atmosphere Community Climate Model: Motivation and Results. *Journal of the Atmospheric Sciences*, *74*(1), 275–291. <https://doi.org/10.1175/JAS-D-16-0104.1>
- Garfinkel, C. I., Hartmann, D. L., & Sassi, F. (2010). Tropospheric Precursors of Anomalous Northern Hemisphere Stratospheric Polar Vortices. *Journal of Climate*, *23*(12), 3282–3299. <https://doi.org/10.1175/2010JCLI3010.1>
- Garfinkel, C. I., Hurwitz, M. M., & Oman, L. D. (2015). Effect of recent sea surface temperature trends on the Arctic stratospheric vortex. *Journal of Geophysical Research: Atmospheres*, *120*, 5404–5416. <https://doi.org/10.1002/2015JD023284>
- Hartmann, D. L. (1981). Some aspects of the coupling between radiation, chemistry, and dynamics in the stratosphere. *Journal of Geophysical Research*, *86*(C10), 9631.
- Hartmann, D. L., & Garcia, R. R. (1979). A Mechanistic Model of Ozone Transport by Planetary Waves in the Stratosphere. *Journal of the Atmospheric Sciences*, *36*(2), 350–364. [https://doi.org/10.1175/1520-0469\(1979\)036<0350:AMMOOT>2.0.CO;2](https://doi.org/10.1175/1520-0469(1979)036<0350:AMMOOT>2.0.CO;2)
- Hoffmann, L., Spang, R., Orr, A., Alexander, M. J., Holt, L. A., & Stein, O. (2017). A decadal satellite record of gravity wave activity in the lower stratosphere to study polar stratospheric cloud formation. *Atmospheric Chemistry and Physics*, *17*(4), 2901–2920. <https://doi.org/10.5194/acp-17-2901-2017>
- Hu, D., & Guan, Z. (2018). Decadal Relationship between the Stratospheric Arctic Vortex and Pacific Decadal Oscillation. *Journal of Climate*, *31*(9), 3371–3386. <https://doi.org/10.1175/JCLI-D-17-0266.1>
- Hu, D., Guan, Z., Tian, W., & Ren, R. (2018). Recent strengthening of the stratospheric Arctic vortex response to warming in the central North Pacific. *Nature Communications*, *9*(1), 1697. <https://doi.org/10.1038/s41467-018-04138-3>
- Hu, D., Guo, Y., & Guan, Z. (2019). Recent weakening in the stratospheric planetary wave intensity in early winter. *Geophysical Research Letters*, *46*, 3953–3962. <https://doi.org/10.1029/2019GL082113>
- Hu, D., Guo, Y., Wang, F., Xu, Q., Li, Y., Sang, W., et al. (2017). Brewer–Dobson Circulation: Recent–Past and Near–Future Trends Simulated by Chemistry–Climate Models. *Advances in Meteorology*, *2017*, 1–13. <https://doi.org/10.1155/2017/2913895>
- Hu, D., Tian, W., Xie, F., Shu, J., & Dhomse, S. (2014). Effects of Meridional Sea Surface Temperature Changes on Stratospheric Temperature and Circulation. *Advances in Atmospheric Sciences*, *31*(4), 888–900. <https://doi.org/10.1007/s00376-013-3152-6>
- Hu, D., Tian, W., Xie, F., Wang, C., & Zhang, J. (2015). Impacts of stratospheric ozone depletion and recovery on wave propagation in the boreal winter stratosphere. *Journal of Geophysical Research: Atmospheres*, *120*, 8299–8317. <https://doi.org/10.1002/2014JD022855>
- Hu, Y., & Tung, K. K. (2003). Possible Ozone-Induced Long-Term Changes in Planetary Wave Activity in Late Winter. *Journal of Climate*, *16*(18), 3027–3038. [https://doi.org/10.1175/1520-0442\(2003\)016<3027:POLCIP>2.0.CO;2](https://doi.org/10.1175/1520-0442(2003)016<3027:POLCIP>2.0.CO;2)
- Huang, B., Thorne, P. W., Banzon, V. F., Boyer, T., Chepurin, G., Lawrimore, J. H., et al. (2017). Extended Reconstructed Sea Surface Temperature, Version 5 (ERSSTv5): Upgrades, Validations, and Intercomparisons. *Journal of Climate*, *30*(20), 8179–8205. <https://doi.org/10.1175/JCLI-D-16-0836.1>
- Hurwitz, M. M., Newman, P. A., & Garfinkel, C. I. (2011). The Arctic vortex in March 2011: a dynamical perspective. *Atmospheric Chemistry and Physics*, *11*(22), 11,447–11,453. <https://doi.org/10.5194/acp-11-11447-2011>

- Hurwitz, M. M., Newman, P. A., & Garfinkel, C. I. (2012). On the influence of North Pacific sea surface temperature on the Arctic winter climate. *Journal of Geophysical Research*, *117*, D19110. <https://doi.org/10.1029/2012JD017819>
- Jadin, E. A., Wei, K., Zyulyaeva, Y. A., Chen, W., & Wang, L. (2010). Stratospheric wave activity and the Pacific Decadal Oscillation. *Journal of Atmospheric and Solar-Terrestrial Physics*, *72*(16), 1163–1170. <https://doi.org/10.1016/j.jastp.2010.07.009>
- Jiang, X., Eichelberger, S. J., Hartmann, D. L., Shia, R., & Yung, Y. L. (2007). Influence of Doubled CO₂ on Ozone via Changes in the Brewer–Dobson Circulation. *Journal of the Atmospheric Sciences*, *64*(7), 2751–2755. <https://doi.org/10.1175/JAS3969.1>
- Kirgis, G., Leblanc, T., McDermid, I. S., & Walsh, T. D. (2013). Stratospheric ozone interannual variability (1995–2011) as observed by lidar and satellite at Mauna Loa Observatory, HI and Table Mountain Facility, CA. *Atmospheric Chemistry and Physics*, *13*(9), 5033–5047. <https://doi.org/10.5194/acp-13-5033-2013>
- Kren, A. C., Marsh, D. R., Smith, A. K., & Pilewskie, P. (2016). Wintertime Northern Hemisphere Response in the Stratosphere to the Pacific Decadal Oscillation Using the Whole Atmosphere Community Climate Model. *Journal of Climate*, *29*(3), 1031–1049. <https://doi.org/10.1175/JCLI-D-15-0176.1>
- Kuroda, Y., & Kodera, K. (1999). Role of planetary waves in the stratosphere-troposphere coupled variability in the northern hemisphere winter. *Geophysical Research Letters*, *26*(15), 2375–2378. <https://doi.org/10.1029/1999GL900507>
- Li, F., Stolarski, R. S., & Newman, P. (2009). Stratospheric Ozone in the Post-CFC Era. *Atmospheric Chemistry and Physics*, *9*(6), 2207–2213. <https://doi.org/10.5194/acp-9-2207-2009>
- Livesey, N. J., Read, W. G., Froidevaux, L., Lambert, A., Manney, G. L., Pumphrey, H. C., et al. (2011). Version 3.3 Level 2 data quality and description document. *JPL D-33509*, 3(2), 4–1.
- Lu, J., Xie, F., Tian, W., Li, J., Feng, W., Chipperfield, M., et al. (2019). Interannual variations in lower stratospheric ozone during the period 1984–2016. *Journal of Geophysical Research: Atmospheres*, *124*, 8225–8241. <https://doi.org/10.1029/2019JD030396>
- Marsh, D. R., Mills, M. J., Kinnison, D. E., Lamarque, J., Calvo, N., & Polvani, L. M. (2013). Climate Change from 1850 to 2005 Simulated in CESM1(WACCM). *Journal of Climate*, *26*(19), 7372–7391. <https://doi.org/10.1175/JCLI-D-12-00558.1>
- Monier, E., & Weare, B. C. (2011). Climatology and trends in the forcing of the stratospheric ozone transport. *Atmospheric Chemistry and Physics*, *11*(13), 6311–6323. <https://doi.org/10.5194/acp-11-6311-2011>
- Nash, E. R., Newman, P., Rosenfield, J. E., & Schoeberl, M. R. (1996). An objective determination of the polar vortex using Ertel's potential vorticity. *Journal of Geophysical Research*, *101*, 9471–9478. <https://doi.org/10.1029/96JD00066>
- Newman, M., Alexander, M. A., Ault, T. R., Cobb, K. M., Deser, C., Di Lorenzo, E., et al. (2016). The Pacific Decadal Oscillation, Revisited. *Journal of Climate*, *29*(12), 4399–4427. <https://doi.org/10.1175/JCLI-D-15-0508.1>
- Newman, P. A., Nash, E. R., & Rosenfield, J. E. (2001). What controls the temperature of the Arctic stratosphere during the spring? *Journal of Geophysical Research*, *106*(D17), 19,999–20,010. <https://doi.org/10.1029/2000JD000061>
- Oman, L. D., Douglass, A. R., Ziemke, J. R., Rodriguez, J. M., Waugh, D. W., & Nielsen, J. E. (2013). The ozone response to ENSO in Aura satellite measurements and a chemistry-climate simulation. *Journal of Geophysical Research: Atmospheres*, *118*, 965–976. <https://doi.org/10.1029/2012JD018546>
- Oman, L. D., Plummer, D. A., Waugh, D. W., Austin, J., Scinocca, J. F., Douglass, A. R., et al. (2010). Multimodel assessment of the factors driving stratospheric ozone evolution over the 21st century. *Journal of Geophysical Research*, *115*, D24306. <https://doi.org/10.1029/2010JD014362>
- Orsolini, Y. J., Karpechko, A. Y., & Nikulin, G. (2009). Variability of the Northern Hemisphere polar stratospheric cloud potential: The role of North Pacific disturbances. *Quarterly Journal of the Royal Meteorological Society*, *135*(641), 1020–1029.
- Randel, W. J. (1987). A Study of Planetary Waves in the Southern Winter Troposphere and Stratosphere. Part I: Wave Structure and Vertical Propagation. *Journal of the Atmospheric Sciences*, *44*(6), 917–935.
- Randel, W. J., Garcia, R. R., Calvo, N., & Marsh, D. (2009). ENSO influence on zonal mean temperature and ozone in the tropical lower stratosphere. *Geophysical Research Letters*, *36*, L15822. <https://doi.org/10.1029/2009GL039343>
- Randel, W. J., Wu, F., & Stolarski, R. (2002). Changes in Column Ozone Correlated with the Stratospheric EP Flux. *Journal of the Meteorological Society of Japan. Ser. II*, *80*(4B), 849–862. <https://doi.org/10.2151/jmsj.80.849>
- Rao, J., Garfinkel, C. I., & Ren, R. (2019). Modulation of the Northern Winter Stratospheric El Niño–Southern Oscillation Teleconnection by the PDO. *Journal of Climate*, *32*(18), 5761–5783. <https://doi.org/10.1175/JCLI-D-19-0087.1>
- Rienecker, M. M., Suarez, M. J., Gelaro, R., Todling, R., Bacmeister, J., Liu, E., et al. (2011). MERRA: NASA's Modern-Era Retrospective Analysis for Research and Applications. *Journal of Climate*, *24*(14), 3624–3648. <https://doi.org/10.1175/JCLI-D-11-00015.1>
- Rood, R. B., & Douglass, A. R. (1985). Interpretation of ozone temperature correlations: 1. Theory. *Journal of Geophysical Research*, *90*(D3), 5733. <https://doi.org/10.1029/JD090iD03p05733>
- Ryan, N. J., Kinnison, D. E., Garcia, R. R., Hoffmann, C. G., Palm, M., Raffalski, U., & Notholt, J. (2018). Assessing the ability to derive rates of polar middle-atmospheric descent using trace gas measurements from remote sensors. *Atmospheric Chemistry and Physics*, *18*(3), 1457–1474. <https://doi.org/10.5194/acp-18-1457-2018>
- Shepherd, T. G. (2008). Dynamics, stratospheric ozone, and climate change. *Atmosphere-Ocean*, *46*(1), 117–138. <https://doi.org/10.3137/ao.460106>
- Shu, J., Tian, W., Austin, J., Chipperfield, M. P., Xie, F., & Wang, W. (2011). Effects of sea surface temperature and greenhouse gas changes on the transport between the stratosphere and troposphere. *Journal of Geophysical Research*, *116*, D02124. <https://doi.org/10.1029/2010JD014520>
- Smith, K. L., Neely, R. R., Marsh, D. R., & Polvani, L. M. (2014). The Specified Chemistry Whole Atmosphere Community Climate Model (SC-WACCM). *Journal of Advances in Modeling Earth Systems*, *6*(3), 883–901. <https://doi.org/10.1002/2014MS000346>
- Solomon, S., Garcia, R. R., & Stordal, F. (1985). Transport processes and ozone perturbations. *Journal of Geophysical Research*, *90*(D7), 12,981–12,989.
- Wallace, J. M., & Gutzler, D. S. (1981). Teleconnections in the Geopotential Height Field during the Northern Hemisphere Winter. *Monthly Weather Review*, *109*(4), 784–812. [https://doi.org/10.1175/1520-0493\(1981\)109<0784:TITGHF>2.0.CO;2](https://doi.org/10.1175/1520-0493(1981)109<0784:TITGHF>2.0.CO;2)
- Weatherhead, E. C., & Andersen, S. B. (2006). The search for signs of recovery of the ozone layer. *Nature*, *441*(7089), 39–45. <https://doi.org/10.1038/nature04746>
- WMO (2014). *Scientific Assessment of Ozone Depletion: 2014, Global Ozone Research and Monitoring Project—Report No. 55*. (p. 416). Geneva, Switzerland: World Meteorological Organization (WMO).
- Woo, S., Sung, M., Son, S., & Kug, J. (2015). Connection between weak stratospheric vortex events and the Pacific Decadal Oscillation. *Climate Dynamics*, *45*(11–12), 3481–3492. <https://doi.org/10.1007/s00382-015-2551-z>
- Xie, F., Li, J., Tian, W., Feng, J., & Huo, Y. (2012). Signals of El Niño Modoki in the tropical tropopause layer and stratosphere. *Atmospheric Chemistry and Physics*, *12*(11), 5259–5273. <https://doi.org/10.5194/acp-12-5259-2012>

- Xie, F., Tian, W., & Chipperfield, M. P. (2008). Radiative effect of ozone change on stratosphere-troposphere exchange. *Journal of Geophysical Research*, *113*, D00B09. <https://doi.org/10.1029/2008JD009829>
- Zhang, J., Tian, W., Xie, F., Chipperfield, M. P., Feng, W., Son, S., et al. (2018). Stratospheric ozone loss over the Eurasian continent induced by the polar vortex shift. *Nature Communications*, *9*(1), 206. <https://doi.org/10.1038/s41467-017-02565-2>
- Zhang, J., Xie, F., Tian, W., Han, Y., Zhang, K., Qi, Y., et al. (2017). Influence of the Arctic Oscillation on the Vertical Distribution of Wintertime Ozone in the Stratosphere and Upper Troposphere over the Northern Hemisphere. *Journal of Climate*, *30*(8), 2905–2919. <https://doi.org/10.1175/JCLI-D-16-0651.1>
- Zhao, X. R., Sheng, Z., Li, J. W., Yu, H., & Wei, K. J. (2019). Determination of the “wave turbopause” using a numerical differentiation method. *Journal of Geophysical Research: Atmospheres*, *124*, 10,592–10,607. <https://doi.org/10.1029/2019JD030754>